Proline-rich Transmembrane protein 2 (PRRT2) controls neuronal excitability by negatively modulating Na^+ channel 1.2/1.6 activity

Floriana Fruscione[1]*, Pierluigi Valente[2]*, Bruno Sterlini[2,3], Alessandra Romei[2,3], Simona Baldassari[1], Manuela Fadda[2], Cosimo Prestigio[2,3], Giorgia Giansante[2], Jacopo Sartorelli[1], Pia Rossi[2], Alicia Rubio[4], Antonio Gambardella[5], Thierry Nieus[6], Vania Broccoli[4], Anna Fassio[2,3], Pietro Baldelli[2,3], Anna Corradi [2,3]*, Federico Zara[1]*, Fabio Benfenati[2,3]*

[1]Laboratory of Neurogenetics and Neuroscience, Istituto Giannina Gaslini, Via Gerolamo Gaslini, 5, 16148 Genova, Italy; [2] Department of Experimental Medicine, University of Genova, Viale Benedetto XV, 3, 16132 Genova, Italy; [3] Center for Synaptic Neuroscience and Technology, Istituto Italiano di Tecnologia, Largo Rosanna Benzi 10, 16132 Genova, Italy; [4] San Raffaele Scientific Institute and National Research Council (CNR), Institute of Neuroscience, Via Olgettina 58, 20132 Milano, Italy, [5]Institute of Neurology, University *Magna Graecia*, Viale Europa, 88100 Catanzaro, Italy; [6] Department of Biomedical and Clinical Sciences "*Luigi Sacco*", University of Milan, Milano, Italy.

* These authors contributed equally to this work

SUPPLEMENTARY MATERIAL

SUPPLEMENTARY METHODS

Plasmids

Lentiviral vectors 743.pCCLsin.PPT.hPGK.GFP.Wpre (a gift from Dr. L. Naldini), FUW–TdTomato (a kind gift from V. Broccoli) were used for iPSC-derived neurons and primary rat neurons infection respectively. For rescue experiments in iPSC-derived neurons, we generated a human PRRT2-Cherry plasmid by cloning the human *PRRT2* sequence (thermo scientific, clone ID 5729288) upstream the Cherry sequence in pm-Cherry vector (Clontech) and subsequently subcloning PRRT2-Cherry into the Age1/Sal1 sites of the lentiviral vector 743.pCCLsin.PPT.hPGK.GFP.Wpre_mut_AMP, replacing the GFP sequence. Likewise, the Cherry sequence was subcloned into the Age1/Sal1 sites of the same plasmid to generate a red variant control (743.pCCLsin.PPT.hPGK.Cherry.Wpre_mut_AMP). For experiments in HEK-293 cell lines, control pKH3 empty vector (a gift from Ian Macara, Addgene plasmid 12555) (Mattingly and Makara, 1996), Tomato fluorescent protein reporter (Clontech), and pKH3-PRRT2-HA vector (PRRT2-HA) (Rossi *et al.*, 2016) were used. For pull down experiment control, we generated pKH3-BAP-HA (BAP-HA) plasmid, by cloning the sequence of bacterial alkaline phosphatase (BAP) upstream the 3xHA sequence into the Hind3 sites of pKH3. To verify the correct orientation DNA sequence was checked.

qRT-PCR and Western blotting

qRT-PCR was performed in a real-time thermal cycler (CFX-96, Bio-Rad) using SsoFast EvaGreen Supermix (Bio-Rad). Total mRNA was extracted with RNeasy mini or micro kit (Qiagen) according to the manufacturer's instructions, and reverse transcribed using the iScript cDNA Synthesis Kit (Bio-Rad). All primers are listed in **Table S1.** Relative expression was calculated using the $2^{-\Delta\Delta Ct}$ method (Pfaffl, 2001) by normalizing data to the geometric mean of three housekeeping transcripts (GAPDH, PPIA, RPL13A) using the CFX Manager 3.0 software (Bio-Rad). For western blotting analysis, protein concentration of the samples was determined using the BCA or Bradford assay and equivalent amounts of protein were subjected to SDS-PAGE on polyacrylamide gels and blotted onto nitrocellulose membranes (Whatman). Blotted membranes were blocked for 1 h in 5% milk in Tris-buffered saline (10 mM Tris, 150 mM NaCl, pH 8.0) plus 0.1% Triton X-100 and incubated overnight at 4°C with the appropriate primary antibody (**Table S2**). Membranes were washed and incubated for 1 h at room temperature with peroxidase-conjugated secondary antibodies. Bands were revealed with the ECL chemiluminescence detection system (ThermoFisher Scientific).

Cell culture and transient transfections

Low-density cortical neurons were prepared from WT and PRRT2-KO mice as previously described (Baldelli *et al.*, 2007; Chiappalone *et al.*, 2006). Animals were sacrificed by CO_2 inhalation, and 17/18-day embryos (E17-18) were removed immediately by cesarean section. In brief, cerebral cortices were dissociated by enzymatic digestion in 0.125% Trypsin for 20 min at 37 °C and then triturated with a fire-polished Pasteur pipette. No antimitotic drugs were added to prevent glia proliferation.

HEK-293 cells stably expressing human $Na_V1.1$, $Na_V1.2$ or $Na_V1.6$ were kind gifts from Drs. Enzo Wanke and Marzia Lecchi (Università di Milano-Bicocca, Italy). HEK-293 cells stably expressing $Na_V1.1$, $Na_V1.2$ or $Na_V1.6$ were maintained in DMEM/F12 (1:1) Glutamax supplemented with 10% fetal bovine serum, 100 units/ml penicillin, 100 µg/ml streptomycin and 500 µg/ml G418 for selection of Na_V channels stably transfected cells. HeLa cells were maintained in DMEM supplemented with10% fetal bovine serum, 1% L-glutamine, 100 units/ml penicillin and 100 µg/ml streptomycin. Cell lines were transfected according to manufacturer's instructions at 80% confluency using Lipofectamine 2000. All reagents were purchased from ThermoFisher Scientific.

Biochemical assays

Pull-down and co-immunoprecipitation. HEK-293 cells stably expressing $Na_V1.1$ or 1.2 or 1.6 subtypes were transfected with PRRT2-HA and BAP-HA as control; after 24 h cells were harvested in lysis buffer (1% Triton X-100, 150 mM NaCl, 50 mM Tris-HCl pH 7.4, with protease inhibitors cocktail). For pull-down assays, 20 µl of monoclonal anti-HA-agarose affinity resin (Sigma-Aldrich) was incubated with cell extract according to manufacturer's instructions for 2 h at 4 °C. After extensive washes in lysis buffer and detergent-free lysis buffer, samples were resolved by SDS-PAGE and subjected to western blotting with polyclonal anti-HA and anti-PanNa_V antibodies. For immunoprecipitation, 5 µg of mouse anti-PanNa_V or mouse control IgGs (anti-GFP and anti-Kv1.2) were precoated with Protein G Sepharose (GE Healthcare) overnight and incubated with a mouse membrane fraction (O'Brien *et al.*, 2012) in lysis buffer. After extensive washes in lysis buffer and detergent-free lysis buffer, samples were resolved by SDS-PAGE and subjected to western blotting with anti-PRRT2 and anti-PanNa_V antibodies.

Surface biotinylation. HEK-293 cells stably expressing $Na_V1.1$ or 1.2 or 1.6 subtypes were transfected with PRRT2-HA plasmids or empty vector pKH3 as a control. Briefly, cells were incubated with 1 mg/ml of EZ-Link™ Sulfo-NHS-SS-Biotin in cold phosphate-buffered saline (PBS) for 40 min at 4 °C, constantly moving. Free biotin was quenched, twice, with 100 mM Tris in cold PBS, and once with cold PBS to remove biotin excess. The cells were then harvested with lysis buffer for 30 min. Whole cell lysates were centrifuged at 16,000 x g at 4 °C for 15 min. 1 mg of the

supernatant was incubated with 100 µl of NeutrAvidin conjugated agarose beads for 3 h at 4 °C, and the remaining supernatant was kept as input. The beads were subsequently washed five times with lysis buffer before elution. All reagents were purchased from ThermoFisher Scientific.

Immunofluorescence

For iPSCs, three germ layer cells and NPCs, staining was performed with PSC 4-MARKER ICC Kit, 3-GERM LAYER ICC Kit and NSC ICC Kit respectively (all from Thermo Fisher Scientific) according to manufacturer's instructions. For iPSC-derived neurons, primary cortical neurons and HeLa cells, IF was performed as previously described (Corradi *et al.*, 2014). PRRT2 staining was performed as previously described (Liu *et al.*, 2016). Antibodies are listed in **Table S2**. All images were taken by a Leica TCS SP8 confocal microscope or by a Zeiss AxioImager M2 microscope and analyzed with ImageJ.

SynaptopHluorin (SypHy) assay

NPCs were transduced with SypHy viral vector (Verstegen *et al.*, 2014) and placed on rat cortical cultures coverslips as previously described for terminal differentiation. Optical recordings of iPSC-derived neurons were performed between 35-40 days of differentiation. Coverslips, immersed in Tyrode solution (140 mM NaCl, 3 mM KCl, 2 mM $CaCl_2$, 1 mM $MgCl_2$, 10 mM HEPES pH 7.4, 10 mM glucose), were put in the stimulation chamber (Warner Instruments) and located on the stage of an IX-81 motorized inverted epifluorescence microscope (Olympus). For Ca^{2+}-free stimulation, Tyrode solution was modified replacing Ca^{2+} with equal molarity of magnesium. An MT20 Hg-Xe lamp (Olympus) was used as light source with 480±20 nm excitation, 495 nm dichroic and 525±50 nm emission filters to detect the GFP signal. Time-lapses were acquired at 1 Hz for 100 s with an Orca-ER IEEE1394 CCD camera (Hamamatsu Photonics) using a UplanSapo 60X1.35 NA oil-immersion objective (Olympus). Cells were maintained in a saline solution at room temperature through a laminar-flow perfusion and the selected field was stimulated after 10 seconds of baseline acquisition. Action potentials were evoked by passing 1-ms biphasic current pulses through platinum-iridium electrodes using a SIU-102 stimulator (Warner Instruments).

Data analysis. Circular ROIs of 1.7 µm diameter were positioned manually at the center of each responsive synapse. Images were analyzed using eXcellence^{RT} software (Olympus). Net fluorescence changes were obtained by subtracting the average intensity of 10 baseline frames (F_0) from the intensity of each frame for individual boutons (ΔF) and then normalizing to the maximum fluorescence intensity (F_{max}) reached under NH_4Cl perfusion ($\Delta F/F_{max}$).

Generation and maintenance of iPSC lines

Cells at low passages (2-3) were reprogrammed using the non-integrating system based on Sendai viruses (CytoTune-iPS reprogramming Kit, Thermo Fisher Scientific) according to manufacturer's instructions. Colonies appeared after 25 days. At least 20 single colonies for each genotype were isolated by manual picking, maintained on Geltrex-coated (Thermo Fisher Scientific) plates on a layer of mitotically inactivated murine embryonic CF-1 fibroblasts (GlobalStem) in hESC culture medium consisting of DMEM/F12 Glutamax supplemented with 20% knockout serum replacement (KSR), 1% non essential amino acids, 1% penicillin/streptomycin, 0.55 mM β-mercaptoethanol and 10 ng/ml recombinant human fibroblast growth factor-2 (FGF-2) (all from Thermo Fisher Scientific). Cultures were fed daily and passaged using collagenase IV every 3–5 days. Each clones was expanded separately as cell lines, which are named in de-identified codes (**Figure S1B**). At passage 15, clones were tested for pluripotency marker expression by qRT-PCR and IF. For in vitro differentiation into cells of all three germ layers, confluent undifferentiated iPSC were incubated in 1 mg ml−1 collagenase IV (Thermo Fisher Scientific) for 1 h at 37 °C and transferred to 100 mm low attachment plates in EB medium (hESC without FGF2). Embryoid bodies (EBs) were grown in suspension for 5–6 days in EB medium and then plated on Geltrex-coated dishes for further 20 days. The medium was changed every 2 days. For virus loss, PCR was performed using primers and instruction as recommended by the manufacturer. All iPSC lines were mycoplasma-free based on tests by the Mycoalert Mycoplasma Detection Kit (Lonza). At least 3 clones from each genotype were kept in culture for further analysis.

Differentiation of iPSC clones into neurons

For neuronal differentiation, embryoid bodies (EBs) were generated as described above (protocol modified from Wen *et al.*, 2014) and cultured for five days in suspension in EB medium and then collected and plated into a Geltrex-coated 6-well plates for additional 7 days to form neural tube-like rosettes in presence of neural induction medium consisting of DMEM/F12, supplemented with N2 (1:100), FGF-2 (20 ng/ml), SB431542 (10 µM; Tocris) and LDN-193189 (0.1 µM; Sigma Aldrich). After 7 days well-formed neural rosettes were picked manually, dissociated completely using Accutase at 37 °C for 10 min and transferred to Geltrex-coated plates in NPC medium consisting of DMEM/F12 supplemented with N2 (1:100), B27 (1:500; GIBCO), epidermal growth factor (EGF; 20 ng/ml) and FGF-2 (20 ng/ml). NPCs were expanded and fed every other day. To obtain terminally differentiated neurons, NPCs infected with GFP expressing lentiviruses (LV) at multiplicity of infection (MOI) of 2 were plated at a concentration of 2.5×10^4 cells/cm^2 onto poly-D-lysine/coated round glass coverslips in co-culture with 1.5×10^4 /cm^2 E18 rat primary cortical neurons at 7 DIV previously infected with TdTomato-LV at MOI 2. The differentiation lasted 25-45

days in Neurobasal-A medium supplemented with 2 mM L-glutamine, B27 (1:50), BDNF (10 ng/ml), GDNF (10 ng/ml) (all from ThermoFisher Scientific) and retinoic acid (1 μM; Sigma-Aldrich) (Shi *et al.*, 2012). Half of the medium was replaced twice a week during continuous culturing.

DNA genotyping and copy number variations (CNVs) analysis

The presence of the PRRT2 mutation was assessed by standard Sanger method. Genomic DNA was extracted from cultured fibroblast and iPSC lines using the QIAmp DNA mini kit (Qiagen) and sequence analysis was performed by 3130 xl Genetic Analyzer (AB Applied Biosystems-Hitachi). Analysis of CNVs has been performed by Array-CGH using Human Genome CGH Microarray kit 8x60K (Agilent^{TM} Technologies) following to manufacturer's protocol. Genomic DNA from each iPSC line and his parental fibroblast were labeled with Cyanine-3 and Cyanine-5 and competitively hybridized on a CGH-array. Data were analyzed using Cytogenomics software with the following analysis settings: aberration algorithm ADM-2; threshold 6.0; window size 0.2 Mb; filter 4 probes, DLRS < 0.25.

Patch-clamp experiments

Patch pipettes, prepared from thin-borosilicate glass (Hilgenberg) were pulled and fire-polished to a final resistance of 2-4 MΩ when filled with standard internal solution. Whole-cell currents were recorded using an EPC-10 amplifier (HEKA Electronic). Voltage-clamp recordings of voltage-gated Na^+ currents and current-clamp recordings investigating single cell firing rates were acquired at 20 kHz and low-pass filtered at 4 kHz, while the AP shape was sampled at 50 kHz and low-pass filtered at 10 kHz. Recordings with leak currents >200 pA or series resistance >20 MΩ were discarded. Data acquisition was performed using PatchMaster program (HEKA Elektronic). R_s was compensated 80% (2 μs response time) and the compensation was readjusted before each stimulation. The shown potentials were not corrected for the measured liquid junction potential of 9 mV. All recordings were performed at 22-24 °C.

Primary cortical neurons and iPSC-derived neurons. Experiments were performed on excitatory cortical neurons morphologically identified by their teardrop-shaped somata and characteristic apical dendrite after 19-21 DIV (Pozzi *et al.*, 2013) and on iPSC-derived neurons between 30 and 45 days of differentiation. For whole cell voltage-clamp of inward/outward currents and current-clamp recordings of firing activity, cells were maintained in Tyrode external solution containing (in mM): 140 NaCl, 2 $CaCl_2$, 1 $MgCl_2$, 4 KCl, 10 glucose, 10 HEPES (pH 7.3 with NaOH). D-AP5 (50 μM), CNQX (10 μM), CGP55845 (10 μM) and bicuculline (30 μM) were added to the external solution on the day of recordings to block NMDA, non-NMDA, $GABA_A$ and $GABA_B$ receptors,

respectively. The standard internal solution was (in mM): 126 KGluconate, 4 NaCl, 1 $MgSO_4$, 0.02 $CaCl_2$, 0.1 BAPTA, 15 glucose, 5 HEPES, 3 ATP, 0.1 GTP (pH 7.2 with KOH). Whole-cell inward/outward currents were elicited using a family of depolarizing 10 ms-voltage steps from -50 to 60 mV and a ramp protocol consisting of a voltage step of 200 ms from the holding potential to -100 mV followed by 100-ms linear ramp up to 120 mV. In both protocols cells were clamped at a holding potential (V_h) of -70 mV before stimulation.

Voltage-clamp recordings of pure voltage-gated Na^+ currents were performed using Tyrode external solution supplemented with $CdCl_2$ (200 μM) to block voltage-gated Ca^{2+} channels. Pipettes were filled with a solution containing (in mM): 4 NaCl, 100 CH_3CsO_3S, 10 TEA-Cl, 5 4-Aminopyridine, 10 EGTA, 1 $CaCl_2$, 10 HEPES, 4 Mg-ATP, 8 Na_2-phosphocreatine (pH 7.4 with CsOH). Neurons, held at -80 mV, were depolarized by a 10-ms voltage pulse at -35/-30 mV to inactivate the out-of-control axonal I_{Na} and isolate the somatic I_{Na}. The latter currents were evoked, after 1 ms at -80 mV, by a series of voltage steps between -80 and +70 mV in 5 mV increments (Milescu *et al.*, 2010; Valente *et al.*, 2016b). Linear capacitance and leakage currents were eliminated by P/N leak subtraction procedure.

HEK-293 cells. HEK-293 cell lines stably expressing human $Na_V1.1$, 1.2 and 1.6 were transfected with 2 μg of PRRT2-HA plasmid or empty vector pKH3 (mock) with Lipofectamine 2000, following the manufacturer's recommendations. To identify transfected cells, a co-transfection with a second plasmid containing the Tomato fluorescent protein reporter (Clontech) was done. Transfected cells were dissociated, re-plated at low density about 24 h post-transfection and recorded after other 24 h. Voltage-clamp recordings of voltage-gated Na^+ currents were performed using the following solutions: extracellular (in mM): 140 NaCl, 3 KCl, 1 $MgCl_2$, 1 $CaCl_2$, 10 HEPES, 10 Mannitol (pH 7.3 with NaOH); intracellular (in mM): 140 CsCl, 10 NaCl, 2 EGTA, 10 HEPES (pH 7.3 with CsOH). Whole-cell family currents of fast inactivating Na_V channels were evoked by 5 mV steps depolarization from -80 to 65 mV and cells were held at -120 mV. Steady-state inactivation curves were constructed by recording the peak currents amplitude evoked by 20-ms test pulses to -10 mV after 500-ms pre-pulses to potentials over the range of -130 to 10 mV. Time-dependent rate of recovery from inactivation was calculated by pre-pulsing the cell with a 20-ms step to -20 mV to inactivate the channels and then bringing back the potential to -100 mV for increasing recovery durations (0.5, 1, 2, 4, 8, 32, 64, 128, 148 ms) before the test pulse of -20 mV. Linear capacity and leakage currents were eliminated by P/N leak subtraction procedure.

Analysis of firing activity. The rheobase was calculated as the minimum depolarizing current needed to elicit at least one action potential. Input resistance was calculated using the Ohm law in the linear region of the voltage-current relationship determined after injection of hyperpolarizing and depolarizing current steps (-10, -10, 10, 20 pA). For each recorded cell, the plot of the time

derivative of voltage (dV/dt) versus voltage (phase-plane plot) was constructed from the first action potential elicited by the minimal current injection. This plot was used to extract threshold potential, maximum rising slope and peak potential (V_{max}). Amplitude of APs was calculated as the difference between the V_{max} and the threshold value. The instantaneous firing frequency and the mean firing frequency were determined at the minimal value of injected current able to evoked two or more APs. The instantaneous firing frequency was estimated as the reciprocal value of the time difference between the first two evoked APs. The mean firing frequency was calculated as the ratio of the number of APs evoked by the minimal current injection to the time interval (in s) between the first and the last evoked action potential (Valente *et al.*, 2016b). Firing activity was also studied using trains of 5 ms-steps applied at various frequencies (10-120 Hz). The current value used to evoked APs with this protocol was selected as the minimal current able to evoke an AP for each step of the train at 10 Hz (100% of probability) and increased by 100 pA.

Analysis of Na^+ currents. The Na^+ current density (J) was obtained by dividing the peak inward current by the cell capacitance (nA/pF). The conductance/voltage relationship (G-V) curves were obtained by converting the maximal current values, evoked with the voltage step protocols, to conductance using the relation $G_{Na}=I_{Na}/(V-V_R)$, where G_{Na} is the Na^+ conductance, I_{Na} is the peak Na^+ current, V is the command pulse potential, and V_R is the theoretical reversal potential of Na^+ current. The normalized activation and inactivation curves for each cell were fitted to the Boltzmann equation in the form: $Y=1/\{1+\exp[(V-V_{0.5})/k]\}$, where Y is the normalized G_{Na} or I_{Na}, V the is the command pulse potential, $V_{0.5}$ is the voltage required to activate the half-maximal conductance or inactivation, and k is the slope of curve.

Modeling of Na^+ currents. We adopted a detailed biophysical model of the Na^+ current (Magistretti *et al.*, 2006), that can be downloaded from the Senselab website (https://senselab.med.yale.edu/) with the accession number 116835. The model was assumed as the control condition of our data (mock). In order to reproduce the leftward shift of the inactivation curve and the unchanged activation curve observed in the presence of PRRT2, we modified the entry and exit rates from the inactivated states. More specifically, we modified the rates as follows: C_{on} from 0.005 to 0.05; O_{off} from 0.005 to 0.00125; and $V0_{theta}$ from 25 to 30. The changes of the first two rates (C_{on} and O_{off}) account for the PRRT2-induced leftward shift of the inactivation curve, while the change in $V0_{theta}$ guarantees the activation curve of remains almost unchanged, at low voltages, in the presence of PRRT2. Further details on the model and on its parameters can be found in Magistretti *et al.*, 2006.

All the electrophysiological data were analyzed using the FitMaster software (HEKA Elektronic), OriginPro 8 (OriginLab Corp.) and the Prism software (GraphPad Software, Inc.).

Analysis of network activity on multielectrode arrays

Preparation of dissociated primary cortical cultures. The day before neuronal culture preparation, planar multi-well MultiElectrode Arrays (MEAs) were coated by depositing 20 µl drop of poly-L-lysine (0.1 mg/ml; Sigma-Aldrich) over each recording area and subsequently incubated overnight. After thorough washing, dissociated cortical neurons prepared from E17 WT and PRRT2-KO embryos were plated at a final density of 80,000 neurons per well. After plating, cells were incubated with 1% Glutamax, 2% B27, 1% penicillin-streptomycin supplemented Neurobasal medium. Half-volume replacement of the culture medium was performed every week. Spiking activity from cortical networks grown onto MEAs was recorded and monitored using Axion BioSystems hardware (Maestro amplifier and Middle-man data acquisition interface) and the software Axion's Integrated Studio (AxIS 2.1). After 1200x amplification, raw data were digitized at 12.5 KHz/channel and stored on a hard disk for subsequent offline analysis.

Recording and stimulation protocols. Experiments were performed at various developmental stages (ongoing synaptogenesis, DIV 14; mature synaptic connections, DIV 21), in culture medium maintained at 37 °C. MEA plates were set on the Maestro apparatus and their spontaneous activity recorded for 15 min, starting 10 min after the transfer to let the culture reach a stable level of activity. On the last day of recording, the spontaneous activity was monitored for 20-30 min before applying electrical stimulation. For pulse stimulation, one electrode was chosen among 64 possible stimulation sites based on visual inspection of the evoked responses to ensure maximal activation of the network. Only the electrodes recording spiking activity were chosen as stimulation sites. Test stimuli were sent to the selected electrode at 0.2 Hz frequency. Pulse stimulation was biphasic with 1.5-V peak-to-peak amplitude, 500 µs duration, and 50% duty cycle (Wagenaar *et al.*, 2004).

In the experiments examining the role of $Na_V1.2$ and $Na_V1.6$ in the increased recurrent activity for PRRT2-KO cultures, mutant and WT primary cortical neurons were grown onto 48-wells MEA chips (Axion BioSystems M768-tMEA-48W). Cultures were tested at DIV 21. After stable occurrence of reverberant network activity, we recorded spontaneous activity for 15 min, before the addition of 1 nM phrixotoxin-3 and 10 nM 4,9-anhydrotetrodotoxin (both from Tocris Bioscience) to block $Na_V1.2$ and $Na_V1.6$, respectively. After 10 min re-equilibration, recordings continued for 15 min. The optimal toxins' concentrations in the IC50 range were tested in preliminary experiments with WT neurons. Drug dilutions were made immediately prior to the experiments, from stock water solutions.

Signal processing for primary cortical neurons cultured on MEAs. Primary neuronal networks show both random spiking activity and bursting behavior (Opitz *et al.*, 2002). Spike detection and spike train data analysis were both computed using the Axion BioSystems software. Single extracellular action potentials were detected running a voltage-threshold-based algorithm over 200

Hz highpass filtered traces; the voltage threshold was 7x the standard deviation of the rms-noise on each channel. No spike sorting procedure was carried out and spike trains were analyzed only by considering multi-unit activity. Bursts within single channels were identified by applying an interspike interval (ISI) threshold algorithm (Chiappalone *et al.*, 2005) by defining bursts as collections of a minimum number of spikes (N_{min} = 5) separated by a maximum interspike interval (ISI_{max} = 100 ms). Network bursts represent the peculiar activity pattern of mature neuronal cultures, consisting of periods of array-wide coherent spiking typically lasting several hundreds of milliseconds and separated by windows of lesser activity (Maeda *et al.*, 1995). Network activity within WT and PRRT2-KO cultures was detected by running an ISI algorithm similar to that applied for burst detection: it identifies a network burst only when a minimum number of spikes (N_{min} = 10) occurs on at least 25% of the electrodes and it is set to automatically estimate the ISI_{max} (Bakkum *et al.*, 2014). Thereafter, from the identified bursts and network bursts, several parameters (e.g. duration, firing rate within burst, average number of spikes per burst, burst frequency) were extracted by means of the Axion Biosystems software NeuralMetric Tool 2.0.4. Instantaneous firing rate and relative parameters (i.e. mean peak firing rate and latency to the peak) were calculated with custom-made algorithms created in Python. Furthermore, to assess the degree of synchronization across the networks, we calculated the Synchrony Index (Paiva *et al.*, 2010), a unitless parameter ranging from 0 to 1 where values close to 1 indicate greater synchrony. When stimulating, currents/voltages are delivered through one electrode of the array at a constant frequency, the network responds by generating a rich repertoire of reverberating electrical activities, lasting 100-200 ms (Shahaf and Marom, 2001). We used PSTHs to investigate the neuronal activity evoked by the electrical stimulation. The PSTHs for each electrode were calculated by averaging the spiking activity recorded over 50 consecutive stimulations on a 200-ms period after each stimulus, prior blanking of the first 2 ms of the response to circumvent stimulation artifacts. Then, the number of spikes occurring in each 5 ms bin was calculated to generate a cumulative histogram that was subsequently normalized by the total number of stimuli and the bin size (Rieke *et al.*, 1997). Evoked activity was analyzed using MathLab (The Mathworks, Natick, MA, USA) and Neuroexplorer (Nex Technologies, Littleton, MA, USA).

References

Bakkum DJ, Radivojevic M, Frey U, Franke F, Hierlemann A, Takahashi H. Parameters for burst detection. Front Comput Neurosci. 2014; *7*: 1-12.

Baldelli P, Fassio A, Valtorta F, Benfenati F. Lack of synapsin I reduces the readily releasable pool of synaptic vesicles at central inhibitory synapses. J Neurosci. 2007; 27: 13520-13531.

Chiappalone M, Novellino A, Vajda I, Vato A, Martinoia S, van Pelt J. Burst detection algorithms for the analysis of spatio-temporal patterns in cortical networks of neurons. Neurocomputing 2005; 65/66: 653-662.

Corradi A, Fadda M, Piton A, Patry L, Marte A, Rossi P, et al. SYN2 is an autism predisposing gene: loss-of-function mutations alter synaptic vesicle cycling and axon outgrowth. Hum Mol Genet. 2014; 23: 90-103.

Maeda E, Robinson HPC, Kawana A. The mechanisms of generation and propagation of synchronized bursting in developing networks of cortical neurons. J Neurosci. 1995; 15: 6834-6845.

Mattingly RR, Macara IG. Phosphorylation-dependent activation of the Ras-GRF/CDC25Mm exchange factor by muscarinic receptors and G-protein beta gamma subunits. Nature 1996; 382: 268-272.

Milescu LS, Bean BP, Smith JC Isolation of somatic Na^+ currents by selective inactivation of axonal channels with a voltage prepulse. J Neurosci. 2010; 30: 7740-7748.

O'Brien JE, Meisler MH Sodium channel SCN8A (Nav1.6): properties and de novo mutations in epileptic encephalopathy and intellectual disability. Front Genet. 2013; 4:213.

Opitz T, De Lima AD, Voigt T. Spontaneous development of synchronous oscillatory activity during maturation of cortical networks in vitro. J Neurophysiol. 2002; 88: 2196-2206.

Paiva ARC, Park I, Principe JC. A comparison of binless spike train measures. Neural Comput Applicat. 2010; 19: 405-419.

Pfaffl MW. A new mathematical model for relative quantification in real-time RT-PCR. Nucleic Acids Res. 2001; 29**:** e45.

Pozzi D, Lignani G, Ferrea E, Contestabile A, Paonessa F, D'Alessandro R, et al. REST/NRSF-mediated intrinsic homeostasis protects neuronal networks from hyperexcitability. EMBO J. 2013; 32: 2994-3007.

Rieke F, Warland D, de Ruyter van Steveninck R, Bialek, W. Spikes: exploring the neural code. (MIT Press, Cambridge, Massachusetts) 1997.

Rossi P, Sterlini B, Castroflorio E, Marte A, Onofri F, Valtorta F. A novel topology of Proline-rich Transmembrane Protein 2 (PRRT2): hints for an intracellular function at the synapse. J Biol Chem. 2016; 291: 6111-6123.

Shahaf G, Marom S. Learning in networks of cortical neurons. J Neurosci. 2001; 21: 8782-8788.

Verstegen AM, Tagliatti E, Lignani G, Marte A, Stolero T, Atias M, et al. Phosphorylation of synapsin I by cyclin-dependent kinase-5 sets the ratio between the resting and recycling pools of synaptic vesicles at hippocampal synapses. J Neurosci. 2014; 34: 7266-7268.

Wagenaar DA, Pine J, Potter SM. Effective parameters for stimulation of dissociated cultures using multi-electrode arrays. J Neurosci Meth. 2004; 138: 27-37.

Table S1. List of the mouse and human primers used for qRT-PCR

Gene Name	Forward	Reverse	Accession number
mouse PRRT2	CCACAATGTTGACAGGCCAC	GAAGGCACCCAGAAACCTCG	NM_001102563
mouse SCN1a	TGTTCGCTTCAAAAGGTGGC	ACGCAAACAAGAGGAGGTGT	NM_001313997
mouse SCN2a	TGTATCTCCAACCACACAACCA	TCTCCACACTGCTGCCTATG	NM_001099298
mouse SCN8a	AGGCCCCGACAGTTTCAAG	GGGTGGTTTCTTGAGCTTGC	NM_001077499
mouse GAPDH	GGCATCGAAGGTGGAAGAGT	GGCATCTTGGGCTACACTGA	NM_001289726
mouse PPIA	TCCTGGCATCTTGTCCATGG	TTCAGTCTTGGCAGTGCAGA	NM_008907
mouse RPL13A	TCCGATAGTGCATCTTGGCC	AAGTACCAGGCAGTGACAGC	NM_009438
human Oct 4	GAGAAGGATGTGGTCCGAGT	GTGCATAGTCGCTGCTTGAT	NM_002701
human SOX2	ACCAGCTCGCAGACCTACAT	CCTGCTGCGAGTAGGACAT	NM_003106
human TDGF1	GGATACCTGGCCTTCAGAGA	CAGGCAGCAGGTTCTGTTTA	NM_001174136
human FGF4	CTCTATGGCTCGCCCTTCT	TGTAGGACTCGTAGGCGTTG	NM_002007
human DPPA2	CATGCTTACCCTGAACAACG	GAAGCCTTGCTCTCTTGGTC	NM_138815
human DPPA4	GAAGAGGATCAGCAGGCTTC	GTTGTCAGTGTGCTCTGCCT	NM_018189
human NANOG	TGTCTTCTGCTGAGATGCCT	AATAAGCAGATCCATGGAGGA	NM_024865
human REX	GGCCTTCACTCTAGTAGTGCTCA	CTCCAGGCAGTAGTGATCTGAGT	NM_174900
human NESTIN	CAGAGGTGGGAAGATACGGT	AGCTCTGCCTCATCCTCATT	NM_006617
human SOX1	TCCTGGAGTATGGACTGTCCG	GAATGCAGGCTGAATTCGG	NM_005986
human PAX6	GATAACATACCAAGCGTGTCATCAATA	TGCGCCCATCTGTTGCT	NM_000280
human PRRT2	GCCAGATTCCCAGCCTAC	GGTCCTCCTGGGTAGGGA	NM_145239
human SCN1A	GGAGGGTGAGGGGCAATA	AGTGGAGGTGCTTTGTTGATCT	NM_001165963
HUMAN SCN2A	TGGGAAGCCATATATCAGTGGT	ATGTTTGTACAGTCGGGCTTTT	NM_021007
HUMAN SCN8A	CTGCAACCAACGTAAACCTGTA	AGCAACAAACACACCAAGACAG	NM_014191
human PPIA	GGAGGCTTTGAGGTTTTGCAA	CCTGACATCTAACTGCCAGCA	NM_021130
human RPL13A	TGAAAGCACTCGGAGAATTG	ACAAGATAGGGCCCTCCA	NM_012423
human GAPDH	AGCAAGAGCACAAGAGGAAGAG	TAACTGGTTGAGCACAGGGTAC	NM_002046

Table S2. List of the primary and secondary antibodies used in the study

Primary Antibodies	Host	Manufacture	Identifier	Diluition	Application
Actin	mouse	Sigma-Aldrich	A4700	1:2000	WB
AFP	mouse IgG1	Thermo Fisher Scientific	A25230	1:500	IF
AnkyrinG	rabbit	Santa Cruz	SC-28561	1:200	IF
Cherry	mouse	Clontech	632543	1:200	WB
GABA	rabbit	Sigma-Aldrich	A2052	1:3000	IF
GAD65	guinea pig	Synaptic systems	198104	1:100	WB,IF
GFP	guinea pig	Synaptic systems	132 005	1:1000	IF
GFP	mouse	Millipore	MAB3580	1:1000	IF, IP
HA	rabbit	Thermo Fisher Scientific	715500	1:1000	WB
Homer1	mouse	Synaptic systems	160011	1:250	IF
Kv1.2	mouse	NeuroMab	K14/16	1:1000	WB, IP
Map2	rabbit	Synaptic systems	188003	1:200	IF
Na/K ATPase pump 1	mouse	Merck	5369	1:1000	WB
Nestin	mouse	Thermo Fisher Scientific	A24345	1:100	IF
NeuN	mouse	Millipore	MAB377	1:100	IF
OCT4	rabbit	Thermo Fisher Scientific	A24867	1:100	IF
PanNav	mouse	Sigma-Aldrich	S8809	1:100	IF, IP
Pax6	rabbit	Thermo Fisher Scientific	A24340	1:100	IF
PRRT2	rabbit	Tsai's lab (Liu et al., 2016)		1:500	IF
PRRT2	rabbit	Sigma-Aldrich	HPA01447	1:1000	WB
SMA	mouse IgG2a	Thermo Fisher Scientific	A25531	1:100	IF
SOX1	goat	Thermo Fisher Scientific	A24347	1:100	IF
SOX2	rabbit	Thermo Fisher Scientific	A24339	1:100	IF
SOX2	rat	Thermo Fisher Scientific	A24759	1:100	IF
SSEA4	mouse IgG3	Thermo Fisher Scientific	A24866	1:100	IF
TRA-1-60	mouse IgM	Thermo Fisher Scientific	A24868	1:100	IF
TUJ1	rabbit	Thermo Fisher Scientific	A25532	1:500	IF
Vamp2	rabbit	Synaptic systems	104102	1:500	IF
Vglut1	guinea pig	Synaptic systems	135 304	1:1000	IF

Secondary antibodies	Host	Manufacture	Identifier	Diluition	Application
Alexa Fluor 488 anti mouse	donkey	Thermo Fisher Scientific	A24350	1:250	IF
Alexa Fluor 488 anti goat	donkey	Thermo Fisher Scientific	A24349	1:250	IF
Alexa Fluor 594 anti rabbit	donkey	Thermo Fisher Scientific	A24343	1:250	IF
Alexa Fluor 488 anti rabbit	donkey	Thermo Fisher Scientific	A25535	1:250	IF
Alexa Fluor 488 anti mouse IgG1	donkey	Thermo Fisher Scientific	A25536	1:250	IF
Alexa Fluor 488 anti rat	donkey	Thermo Fisher Scientific	A24876	1:500	IF
Alexa fluor 594 anti mouse IgG2a	goat	Thermo Fisher Scientific	A25534	1:250	IF
Alexa Fluor 594 anti rabbit	goat	Thermo Fisher Scientific	A11037	1:500	IF
Alexa Fluor 594 anti mouse IgG	goat	Thermo Fisher Scientific	A11005	1:500	IF
Alexa Fluor 488 anti mouse IgG3	goat	Thermo Fisher Scientific	A24877	1:500	IF
Alexa Fluor 594 anti mouse IgM	goat	Thermo Fisher Scientific	A24872	1:500	IF
Alexa Fluor 488 anti mouse IgG	goat	Thermo Fisher Scientific	A11029	1:500	IF
Alexa Fluor 546 anti mouse IgG	goat	Thermo Fisher Scientific	A11030	1:500	IF
Alexa Fluor 488 anti guinea pig	goat	Thermo Fisher Scientific	A11073	1:500	IF
Alexa Fluor 647 anti mouse	goat	Thermo Fisher Scientific	A21235	1:500	IF
Alexa Fluor 594 anti guinea pig	goat	Thermo Fisher Scientific	A11076	1:500	IF
Alexa Fluor 647 anti rabbit	goat	Thermo Fisher Scientific	A21244	1:500	IF
Peroxidase conjugated anti-rabbit	goat	Bio-Rad	1706515	1:3000	WB
Peroxidase conjugated anti-mouse	goat	Bio-Rad	1706516	1:5000	WB

SUPPLEMENTARY FIGURES

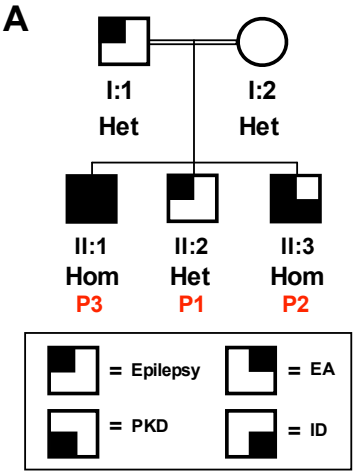

B

Individual	Genotype	Phenotype	Age at onset	Number of Clones (ID)
Control 1 (C1)	Wild type	None	None	3 (**C1.25**; **C1.28**; **C1.32**)
Control 2 (C2)	Wild type	None	None	1 (C2.6)
Patient 1 (P1)	Het c.649dupC	Infantile seizures	4 months	3 (P1.30, P1.35, P1.45)
Patient 2 (P2)	Hom c.649dupC	Infantile seizures, absences, paroxysmal kinesigenic dyskinesia, intellectual disability	3 months	2 (P2.5, P2.18)
Patient 3 (P3)	Hom c.649dupC	Infantile seizures, absences, paroxysmal kinesigenic dyskinesia, episodic ataxia, intellectual disability	4 months	1 (P3.30)

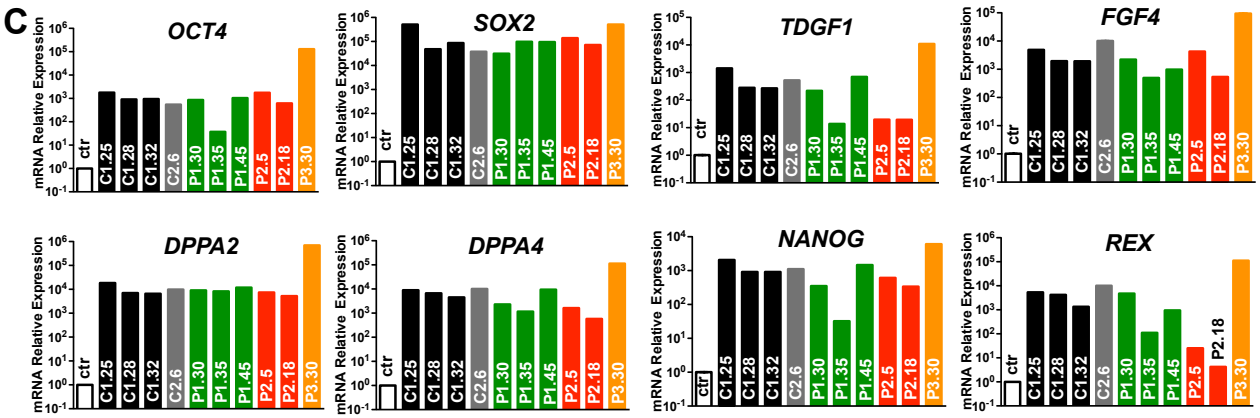

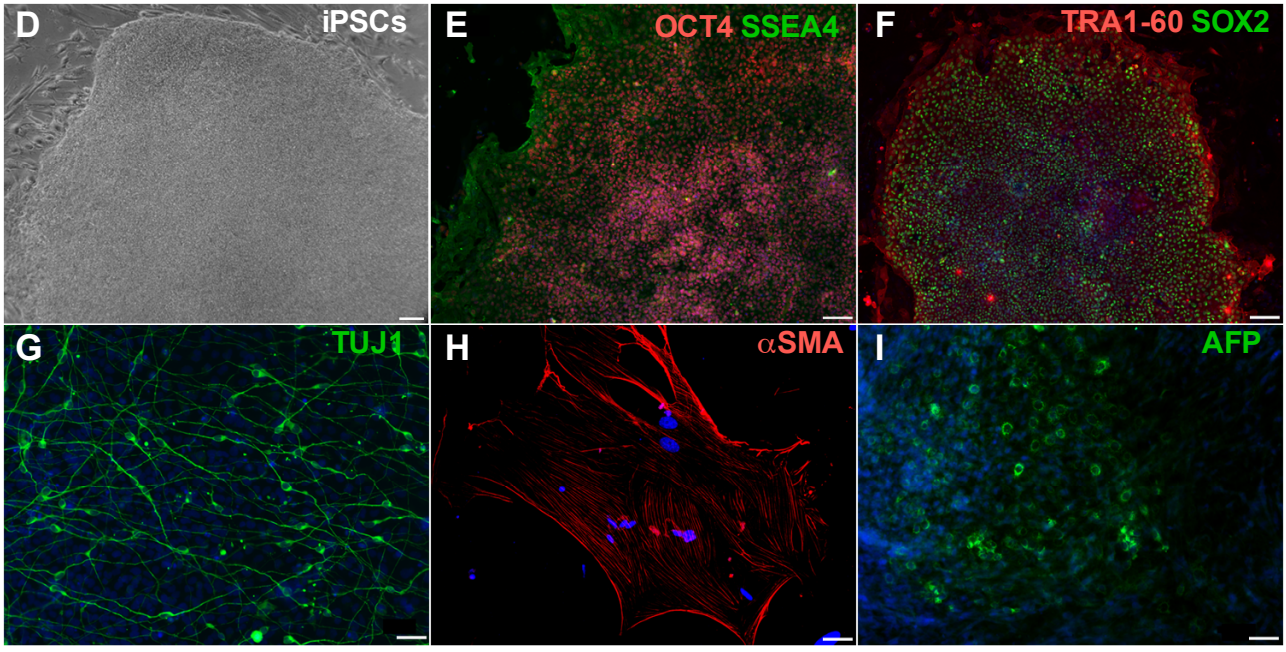

Figure S1. Generation of iPSC lines from fibroblasts of patients carrying the c.649dupC mutation in PRRT2 (related to Figure 1)

A. Pedigree of the consanguineous family segregating the c.649dupC mutation. Heterozygous carriers (I:1, I:2 and II:2/P1) manifest a transient epilepsy in infancy or are asymptomatic. Homozygous carriers (II:1/P3, II:3/P2) show a severe neurological phenotype. PKD, paroxysmal kinesigenic dyskinesia; EA, episodic ataxia; ID, intellectual disability. **B.** Clinical and genetic features of individuals from the consanguineous family segregating c.649dupC (P1-P3) and sex- and age-matched healthy controls (C1,C2). For each individual, the ID of the respective iPSC clones is reported. **C**. Gene expression profile obtained by qRT-PCR showing upregulation of pluripotency-associated genes in iPSC lines (black/gray bars, control clones; green bars, clones from the heterozygous individual; red/orange bars, clones from homozygous individuals). Data are means ± sem (N=3) of relative expression using non-infected fibroblasts from a control (Ctr) as reference (open bars). **D.** Morphology of an iPSC clone at the undifferentiated state. Scale bar, 50 μm. **E,F.** Representative immunofluorescence images showing expression of the pluripotency markers OCT4, SSEA4, TRA-1-60 and SOX2 in iPSC lines. Nuclei were stained with DAPI. Scale bar, 100 μm. **G-I.** iPSC clones generate cells of the three germ layers. Representative immunofluorescence images of *in vitro* differentiated cells expressing ectodermal (TUJ1; **G**), mesodermal (α-SMA; **H**) and endodermal (AFP; **I**) markers. Nuclei were stained with DAPI. Scale bar, 50 μm.

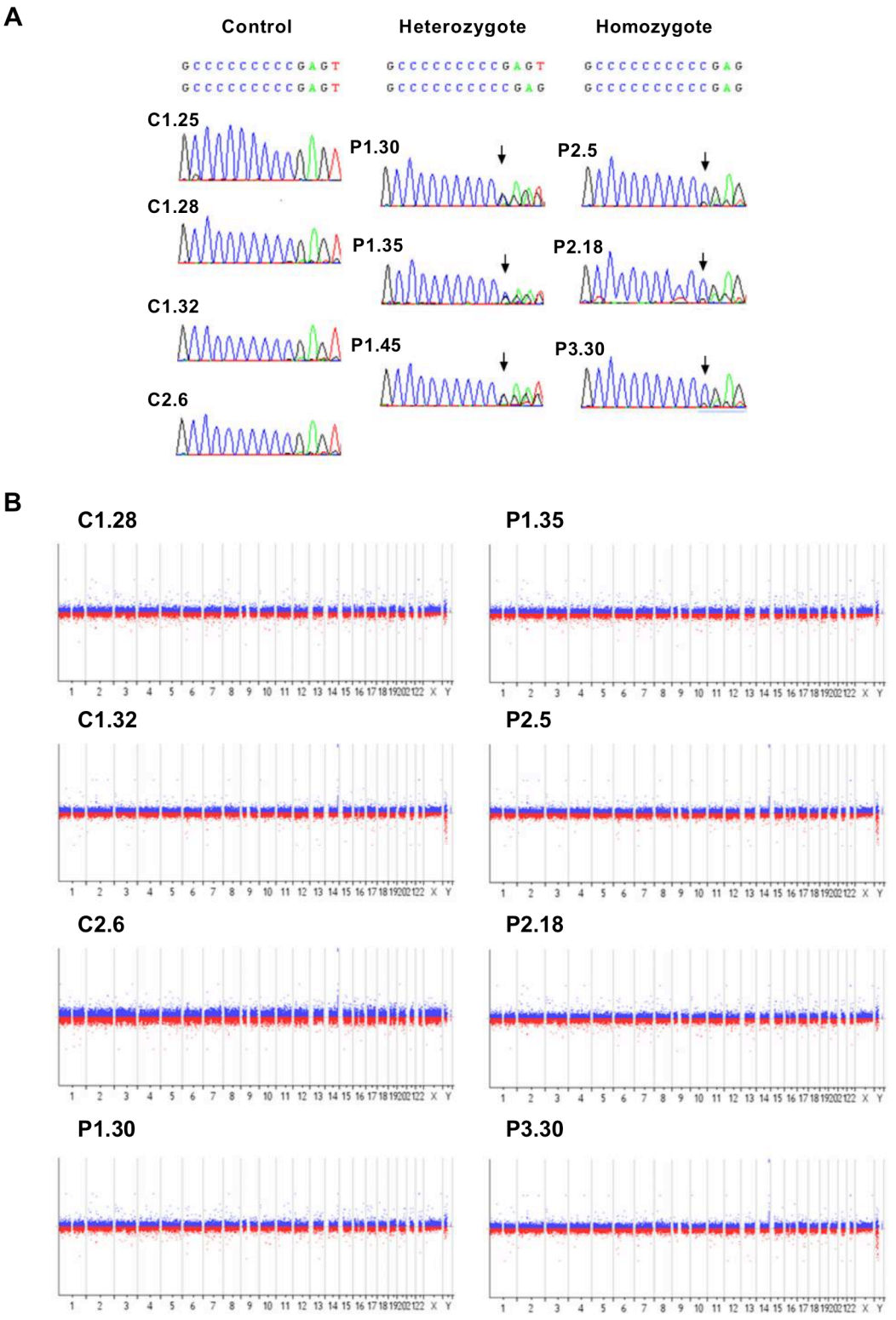

Figure S2. Genetic characterization of iPSC lines from fibroblasts of patients carrying the c.649dupC mutation in PRRT2 (related to Figure 1)

A. Sequencing analysis of c.649dupC mutation in iPSC clones. Clones P1.30, P1.35 and P1.45 from heterozygous patient 1; clones P2.5, P2.18 and P3.30 from homozygous patient 2 and patient 3. iPSC clones from two unrelated non-carrier individuals were also generated (C1.25, C1.28, C1.32 and C2.6) as controls. **B.** Comparative genomic hybridization between genomic DNA of fibroblasts and that of the corresponding iPSC clones. No copy number variations are observed at an average genomic resolution of 75 Kb. A recurrent artifact is found in C1.32, C2.6, P2.5 and P3.30 on chromosome 14q32.3.

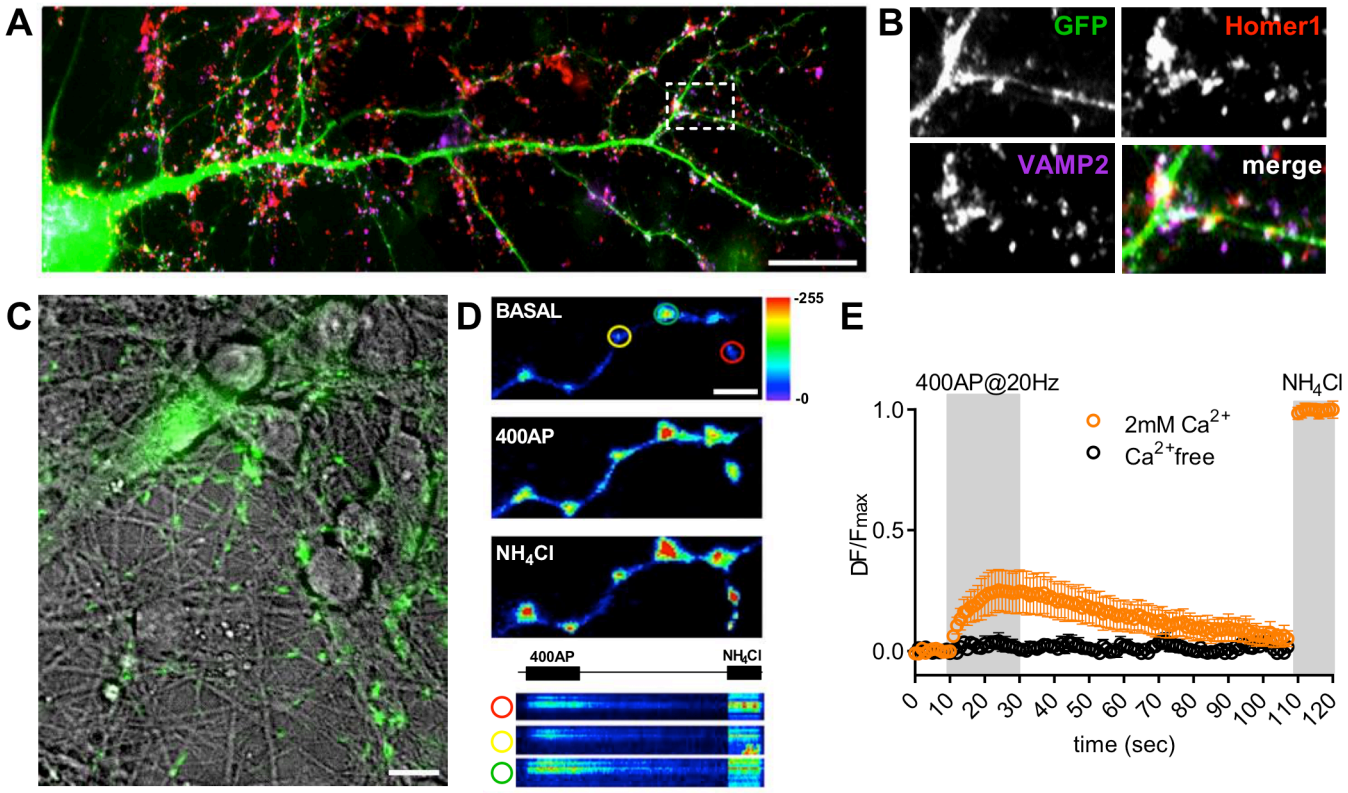

Figure S3. iPSC-derived neurons form active synaptic connections responding to electrical stimulation (related to Figure 1)

A. Representative merge image of cell body and neurites of GFP-infected iPSC-derived neurons (35 days of differentiation) immunostained with anti-VAMP2/synaptobrevin2 and anti-Homer1 antibodies. The white square represents the area sampled in B. Scale bar, 20 µm. **B**. Field magnification of GFP, VAMP2, Homer1 signals. Merge panel shows synaptic contacts along a GFP-positive neurite. **C**. Representative panel with superimposed phase-contrast image and fluorescence images from iPSC-derived neurons infected with SypHy (green) to show positive transduced processes surrounded by the neuronal network. Scale bar, 10 µm. **D**. Representative images of SypHy fluorescence detected at rest (Basal), upon stimulation for 20 sec @ 20 Hz (400 action potentials (AP)) and in the presence of 50 mM NH_4Cl (NH_4Cl). Three representative regions of interest (ROIs) of 1.7 µm diameter (red, green and yellow circles) corresponding to synaptic boutons are shown. The bottom panels show the relative kymographs of fluorescence intensity variation as a function of time for the electrical stimulation and NH_4Cl perfusion. Heat-map scale for pseudo-colored is shown on the right. Scale bar, 5 µm. **E**. Ensemble averaged traces of SypHy fluorescence from iPSC-derived neurons (35 days of differentiation) recorded in response to electrical field stimulation at 20 Hz for 20 s (shaded area) in Tyrode's solution supplemented with 2 mM Ca^{2+} (orange symbols) or in Ca^{2+}-free medium (black symbols). Data demonstrating the Ca^{2+}-dependent synaptic activity in iPSC-derived neurons are normalized to the maximum fluorescence intensity reached under NH_4Cl perfusion ($\Delta F/F_{max}$).

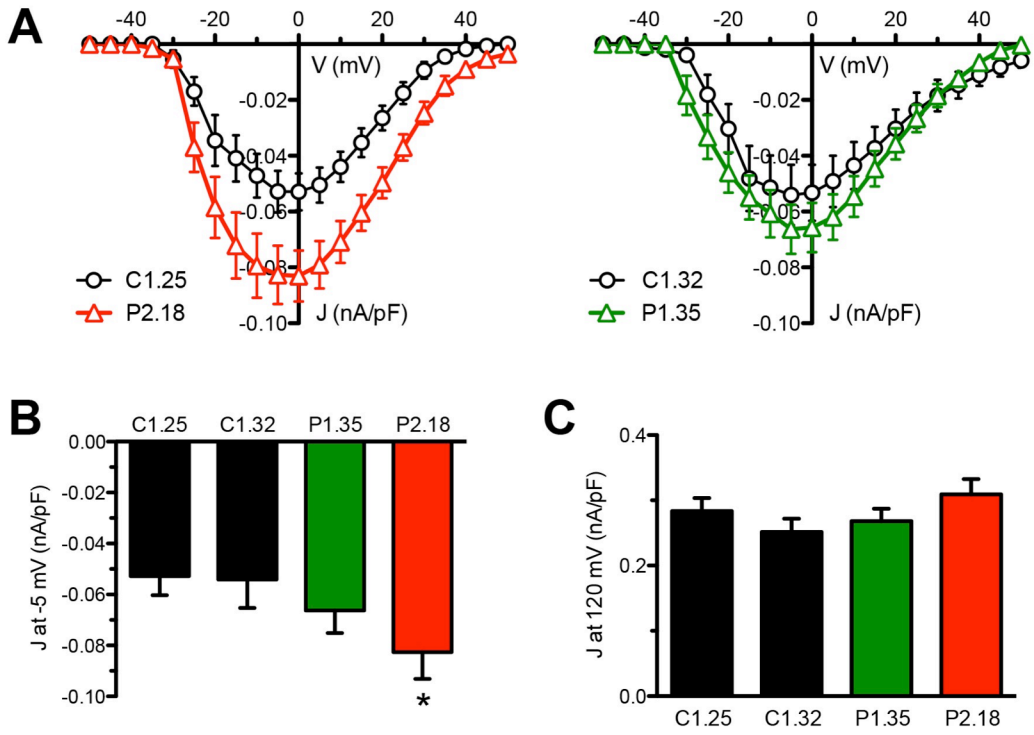

Figure S4. Neurons differentiated from independent iPSC clones from patients and controls show the same inward current phenotype (related to Figure 2)

A. Current density-voltage relationship analyzed in iPSC-derived neurons derived from C1.25 and P2.18 (*left*) and from C1.32 and P1.35 (*right*) iPSC clones, calculated using the voltage-step protocol explained in the text. Clones were grouped in two different panels for clarity. Peak current amplitudes were normalized to the cell capacitance to obtain current density. **B,C.** Quantitative analysis of the current density at -5 (**B**) and 120 (**C**) mV in neurons differentiated from the iPSC clones shown in panel A. The current density at 120 mV (**C**) was studied by the ramp protocol explained in the text. All data are means ± sem. *p < 0.05, Kruskal-Wallis test followed by the Dunn's multiple comparison test *vs* either control (N=22 for C1.25, n=37 for P2.18; N=31 for C1.32; N=24 for P1.35).

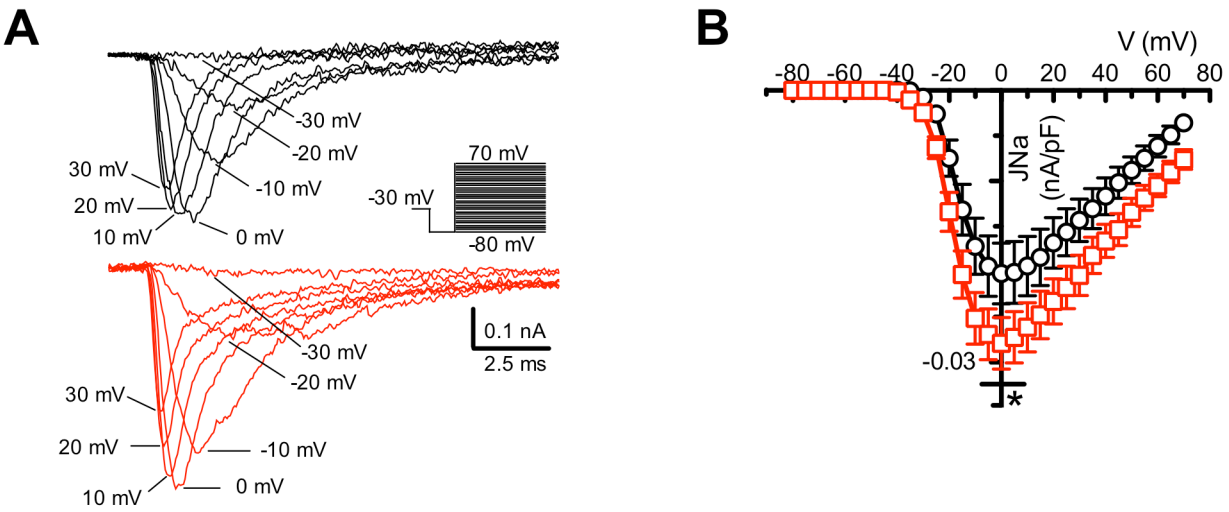

Figure S5. Increase in voltage-gated Na^+ currents in iPSC-derived neurons (related to Figures 2 and 3)

A,B. Representative macroscopic currents (**A**) recorded from C1.28 (black symbols/traces) and P2.5 (red symbols/traces) iPSC-derived neurons and the respective current density *vs* voltage relationship (**B**; means ± sem). Neurons were depolarized by a 10-ms voltage pulse at -30 mV to inactivate the out-of-control axonal I_{Na} and isolate the somatic I_{Na} that were evoked, after 1 ms at -80 mV, by a series of voltage steps between -80 and 70 mV in 5 mV increments (inset). N= 17 and 21 for control and homozygous iPSC-derived neurons, respectively. *p < 0.05, unpaired Student's *t*-test/Mann-Whitney's *U*-test.

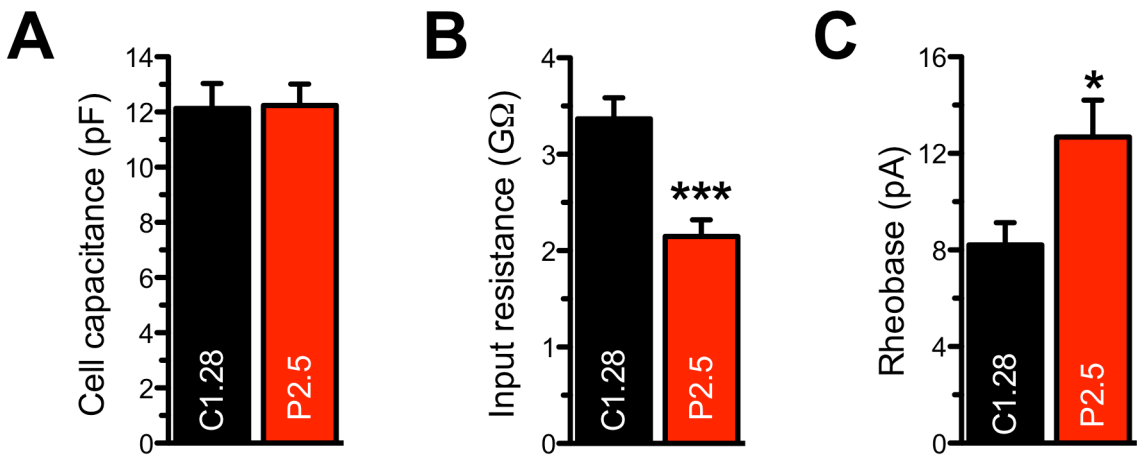

Figure S6. Capacitance, input resistance and rheobase in control and homozygous iPSC-derived neurons (related to Figures 2 and 3)

Cell capacitance (**A**), input resistance (**B**) and the current needed to evoke the first action potential (rheobase; **C**) were calculated in iPSC-derived neurons from control (C1.28) and homozygous (P2.5) genotypes. Data are shown as means ± sem (N=28 for C1.28 and N=33 for P2.5).

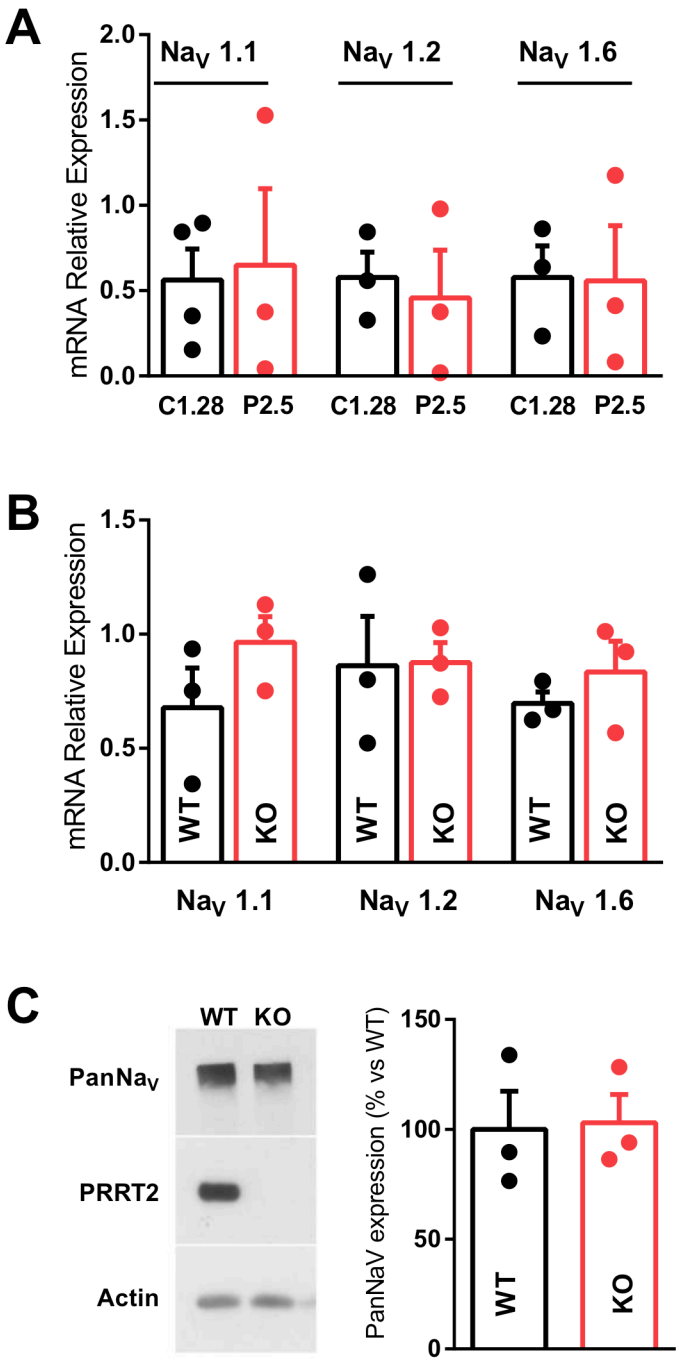

Figure S7. Expression of Na$_V$1.1, Na$_V$1.2 and Na$_V$1.6 channel subtypes in iPSC-derived neurons and mouse PRRT2-KO neurons (related to Figures 2 and 4)

A,B. qRT-PCR.analysis of the expression of human Na$_V$1.1, 1.2 and 1.6 mRNAs in iPSC-neurons derived from C1 control (C1.28) and P2 homozygous patient (P2.5) after 4 weeks of differentiation (**A**), and in primary cortical neurons from WT and PRRT2-KO mice (11-13 DIV; **B**). Data are expressed as means ± sem of N=3 independent preparations. **C.** Expression levels of Na$_V$ channels of WT and PRRT2-KO low-density cortical neurons (15 DIV). Samples were separated by SDS-PAGE and analyzed by immunoblotting with antibodies to PanNa$_V$, PRRT2 and actin. *Left:* a representative immunoblot. *Right:* quantification of the PanNa$_V$ immunoreactive signal calculated in percent of the levels of WT neurons (means ± sem; N=3 independent preparations). No significant differences were observed (Student's *t*-test).

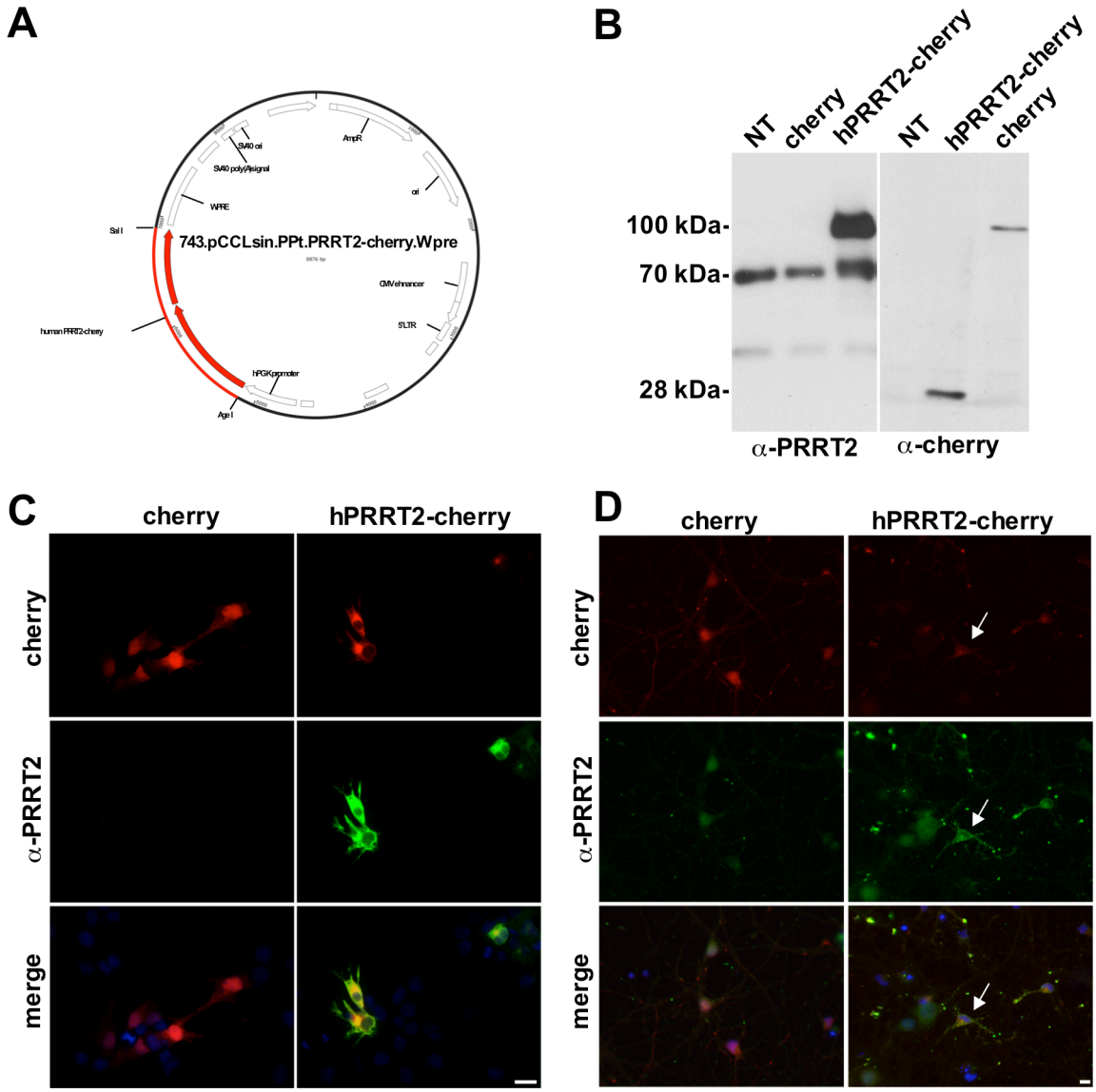

Figure S8. Expression of human PRRT2-Cherry in HeLa cells and primary mouse neurons by lentiviral vectors (related to Figure 3)

A. Map of human PRRT2-Cherry subcloned into the 743.pCCLsin.PPT.hPGK.GFP.Wpre lentiviral vector (a gift from Dr. L. Naldini). **B.** Western blot of lysates of mouse cortical neurons transduced with human-PRRT2-Cherry or control Cherry lentiviruses and probed with anti-PRRT2 (*left*) or anti-Cherry (*right*) antibodies. Transduced neurons express both the PRRT2-Cherry band at 100 kDa and endogenous PRRT2 band (70 kDa). **C.** HeLa cells were transfected with human-PRRT2-Cherry or control Cherry lentiviral plasmids. After 24 h of transfection, the intrinsic Cherry fluorescence (upper panel) and the PRRT2 immunoreactivity (middle panel) were visualized in control Cherry (*left*) or human PRRT2-Cherry (*right*) transfected cells. Merged images from top and middle panels are shown in the bottom panels. Scale bar: 20 μm. **D.** Primary mouse cortical neurons were transduced at 6 DIV with human PRRT2-Cherry or control Cherry lentiviruses. After 5 days of infection, the intrinsic Cherry fluorescence (upper panel) and the PRRT2 immunoreactivity (middle panel) were visualized in control Cherry (*left*) or human PRRT2-Cherry (*right*) transduced neurons. Merged images from top and middle panels are shown in the bottom panels. Scale bar: 10 μm.

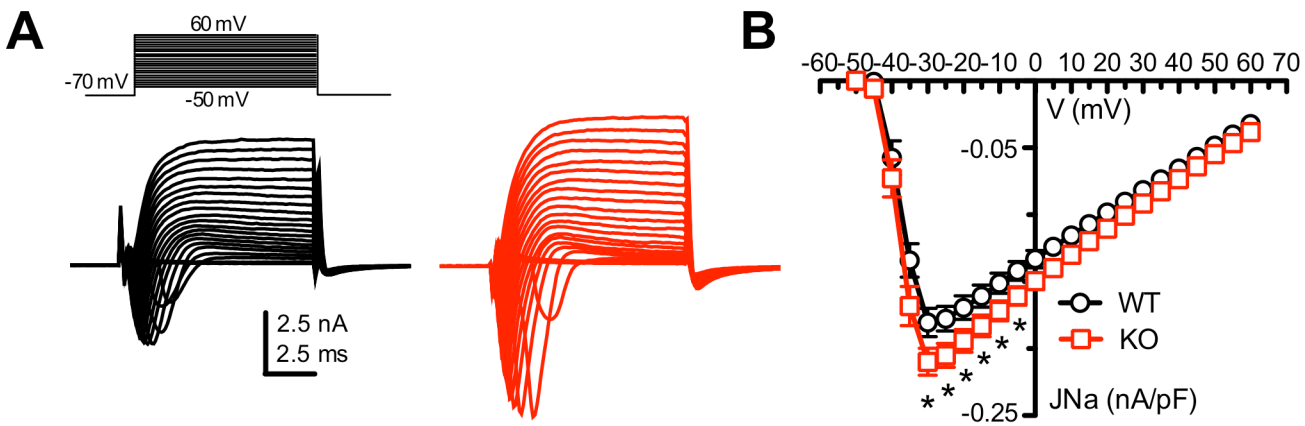

Figure S9. The increase in inward currents in mouse primary neurons (related to Figure 4)
A,B. Representative macroscopic currents (**A**) evoked by either a series of depolarizing voltage steps from -50 to 60 mV (inset) and the inward current density *vs* voltage (J/V) relationship (**B**; means ± sem) calculated, using the protocol shown in A, in WT (black symbols/traces) and PRRT2-KO (red symbols/traces) excitatory cortical neurons. Cells were clamped at -70 mV before stimulation. N= 59 and 64 for WT and PRRT2-KO neurons, respectively.

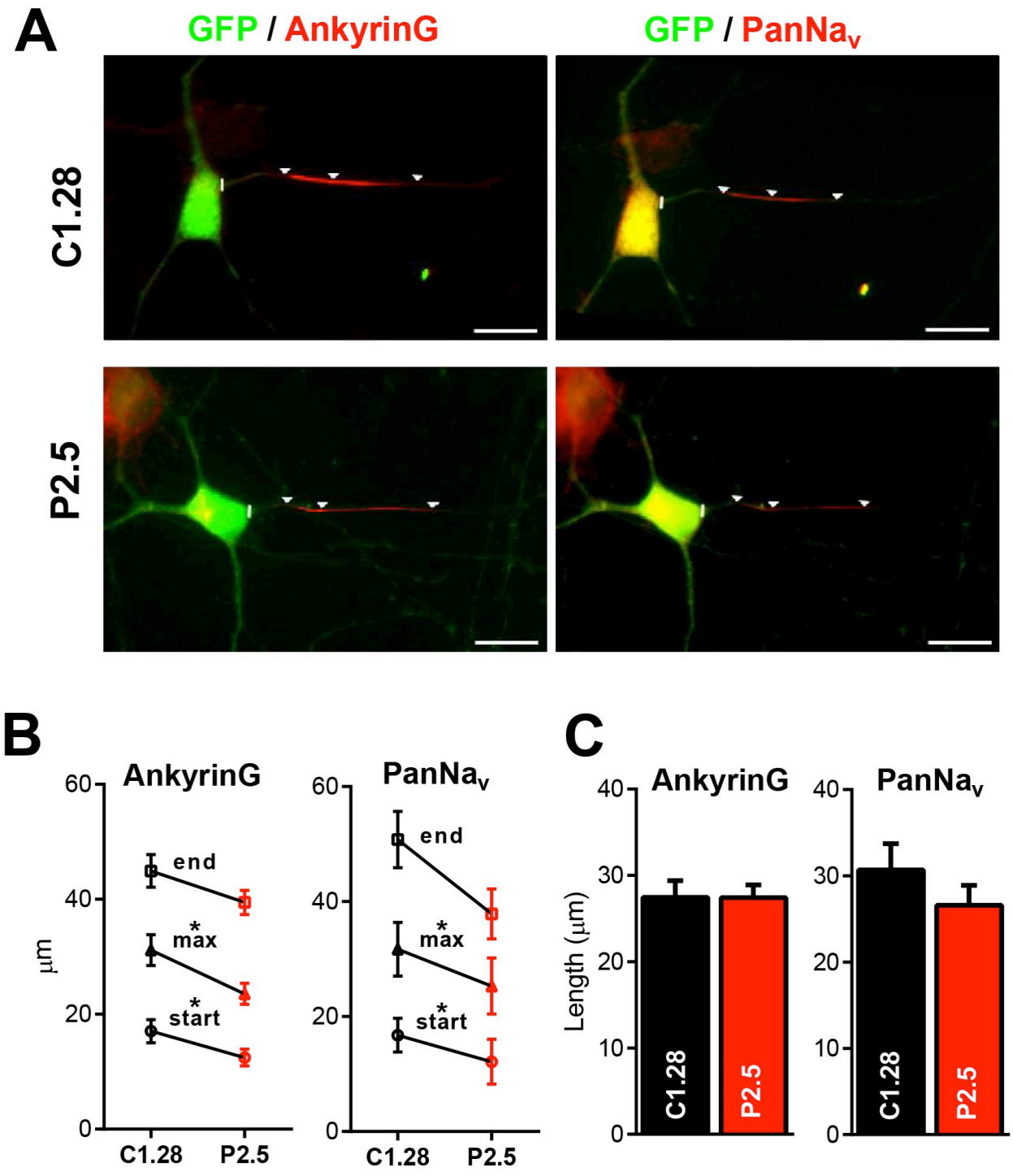

Figure S10. Homozygous iPSC-derived neurons display a proximal shift of the AIS (related to Figure 4)

A. Representative images of GFP-positive C1.28 and P2.5 iPSC-derived neurons immunostained for AnkyrinG and PanNa$_V$. White lines show the axon hillock; arrowheads show the start, maximum and end of the AIS, respectively. Scale bar, 10 µm. **B,C.** Distance of AIS start, maximum and end from the cell body (**B**) and AIS length (**C**) in C1.28 (black) and P2.5 (red) iPSC-derived neurons. Data are shown as means ± sem; N=38 (AnkyrinG) and N=21 (PanNa$_V$) for both C1.28 and P2.5 from N=3 independent experiments. *p<0.05, ***p<0.001; Student's *t*-test/Mann-Whitney *U*-test.

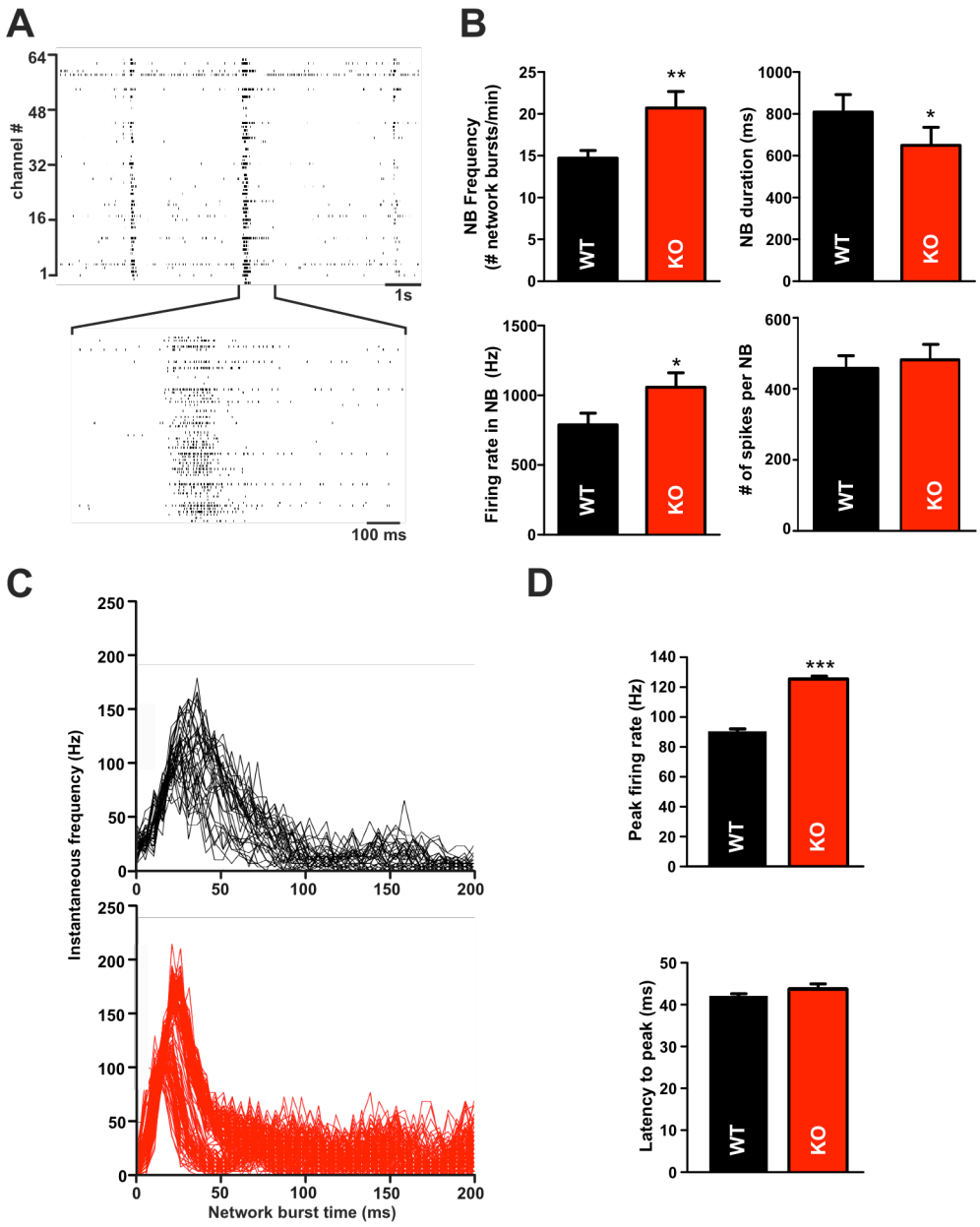

Figure S11. Enhanced network synchronization in mouse PRRT2-KO neuronal networks (related to Figure 5)

A. Raster plot showing 10 s of spontaneous activity in a WT cortical culture during the third week *in vitro*. Both random firing and synchronized activity over a large proportion of active channels is observed. A population burst of APs, typically lasting few hundreds of ms and separated by rare firing, is shown in an enlarged time scale. **B.** Spontaneously generated network bursts (NB) in mature PRRT2-KO (red) and WT (black) cultures were detected through an adaptive ISI-threshold algorithm. Four main parameters were extracted and analyzed: network bursting rate, number of spikes per network burst, network burst duration and mean intraburst firing rate. At equivalent number of spikes per burst, mutant networks displayed significantly shorter bursts and consequently higher intraburst firing rate. **C.** Superimposed instantaneous frequency traces (bin size: 5 ms) of 50 consecutive network bursts measured over a 200 ms-period in representative WT (top) and PRRT2-KO (bottom) cultures. **D.** Temporal analysis of the spiking activity during collective bursting events. The mean peak firing rate for PRRT2-KO was significantly higher than for WT, while the latency to the firing peak was comparable. Data are plotted as means ± sem for WT (black) and KO (red) cultures. N=4 preparations for each genotype; 44 and 46 independent experiments for WT and PRRT2-KO respectively. Mann-Whitney *U*-test for independent samples (*p<0.05, **p<0.01, ***p<0.001).

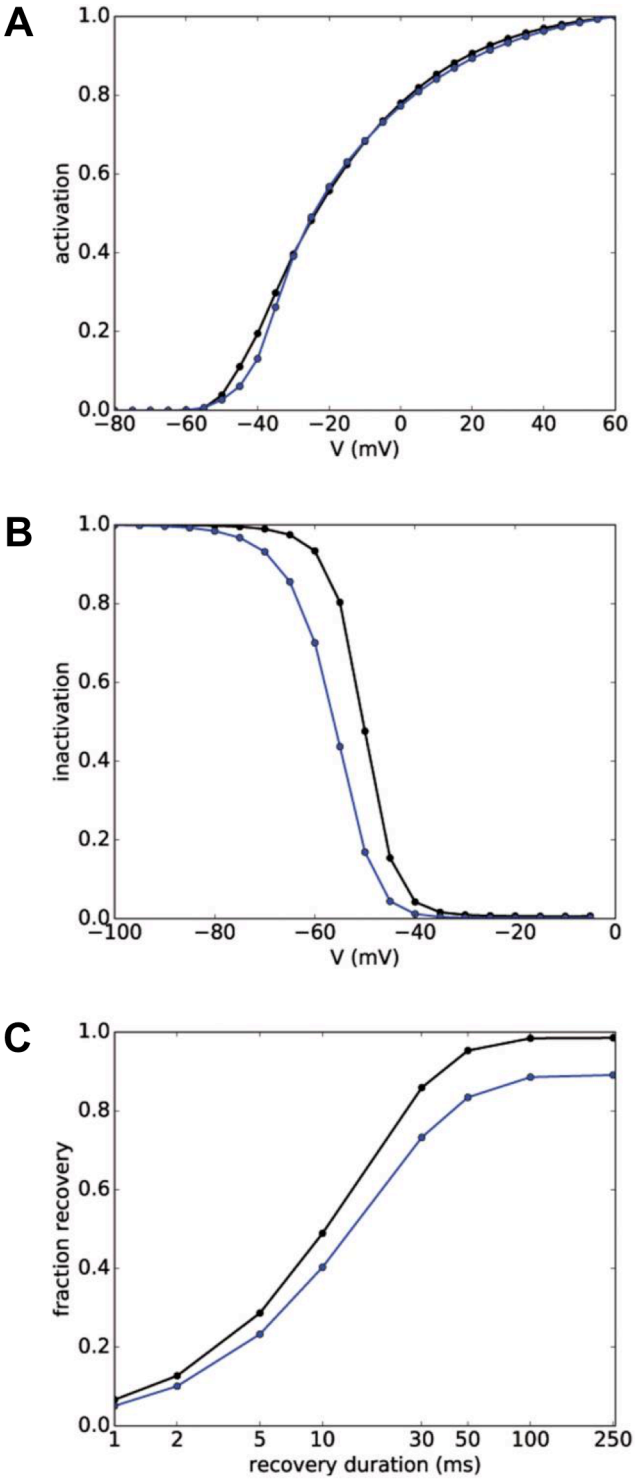

Figure S12. Modeling of the PRRT2-induced changes in voltage-dependent Na^+ channels (related to Figure 6)

Experimental data obtained under control conditions for $Na_V1.2/1.6$ (black traces) were entered in a detailed biophysical model of the Na^+ current. To reproduce the unchanged activation curve and the leftward shift of the inactivation curve observed in the presence of PRRT2 (blue traces), the entry and exit rates of the inactivated state (C_{on}, O_{off}, $V0_{theta}$) were modified as described in the Online Methods. The changes of the first two rates account for the PRRT2-induced leftward shift of the inactivation curve (**B**), while the change in $V0_{theta}$ guarantees that the activation curve remains almost unchanged, at low voltages, in the presence of PRRT2 (**A**). The modeling shows that the leftward shift of the inactivation curve is sufficient to explain the delayed/incomplete recovery from inactivation of the Na^+ current (**C**). Experimental data were taken from main Fig. 6C-E.

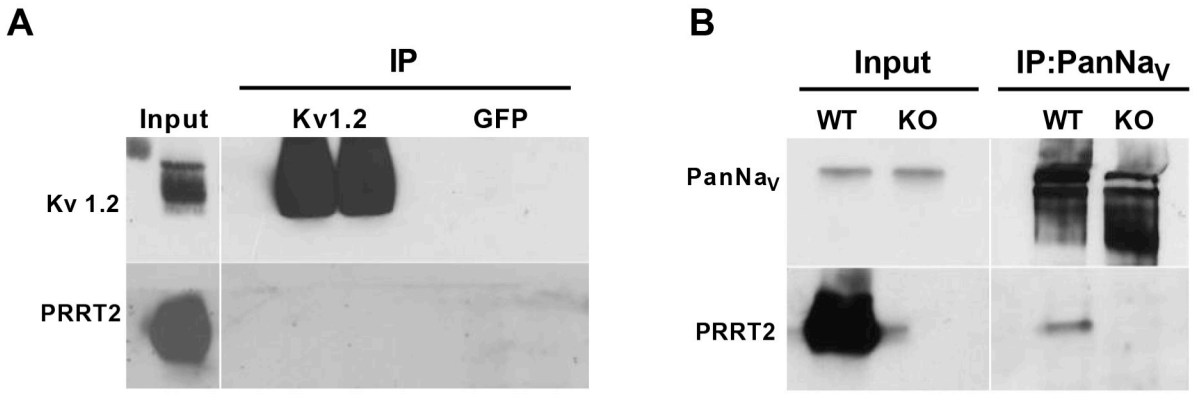

Figure S13. Specificity of the Na_V-PRRT2 co-immunoprecipitation (related to Figure 7)
A. Extracts of a membrane fraction from the whole adult brain from WT or PRRT2-KO mice were used for immunoprecipitation (IP) with anti-Kv1.2 and anti-GFP antibodies. Membranes were probed with anti-Kv1.2 and anti-PRRT2 antibodies as indicated. Input, 50 μg. Control antibodies did not co-precipitate any PRRT2 immunoreactive signal from extract of WT brain. **B.** Extracts of a membrane fraction from the whole adult brain from WT or PRRT2-KO mice were used for the immunoprecipitation (IP) with anti-$PanNa_V$ antibodies described in Figure 7C. Membranes were probed with anti-$PanNa_V$ and anti-PRRT2 antibodies as indicated. Input, 50 μg. No cross-reactive bands were detected in the PRRT2 molecular mass range. Vertical white lines in the blots indicate that the lanes were on the same gel, but have been repositioned in the figure.

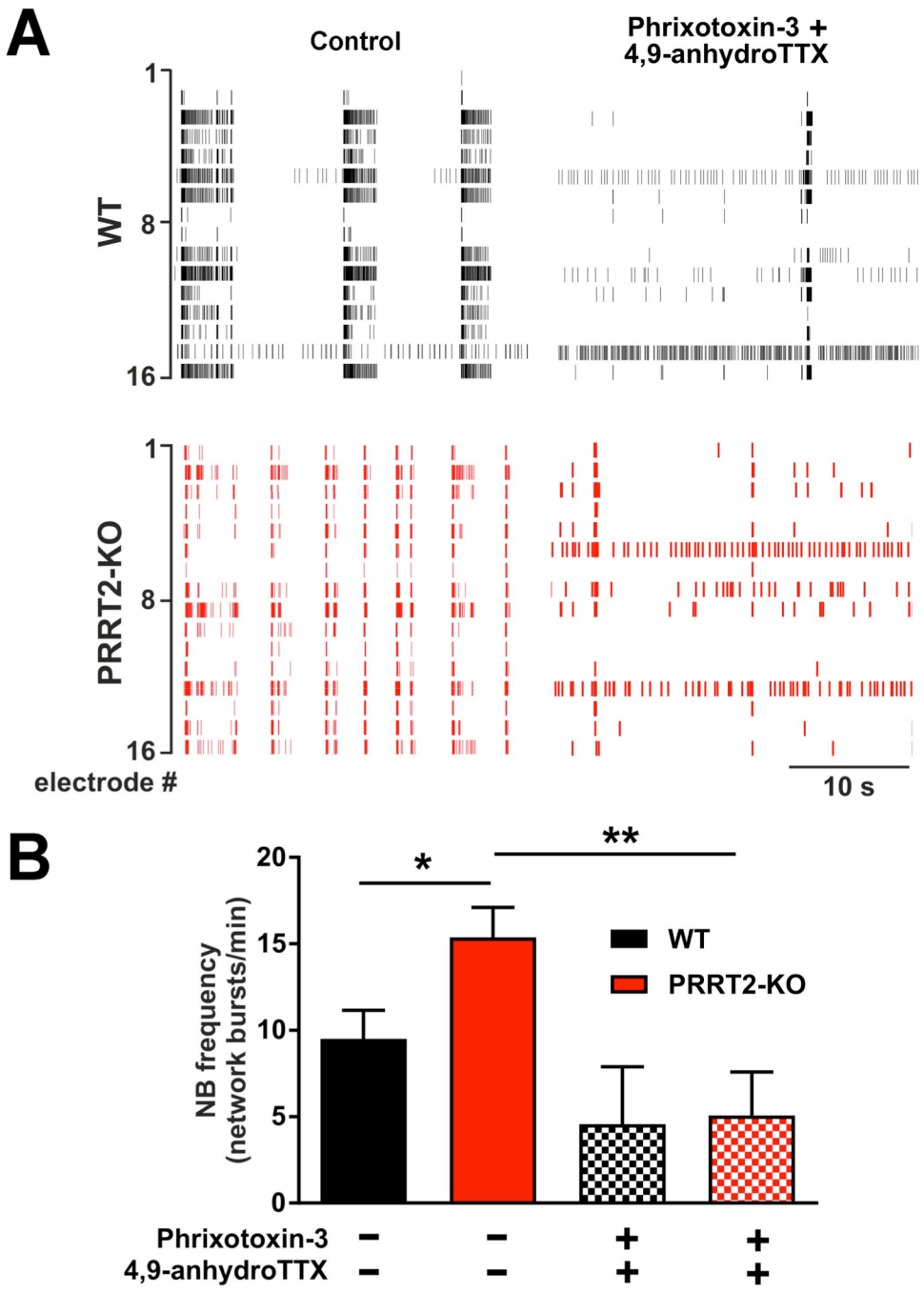

Figure S14. Partial blockade of Nav1.2 and Nav1.6 channels abolishes the genotype-dependent differences in network bursting rate (related to Figure 7)

A. Raster-plots indicating firing events recorded on each of the 16 channels for representative WT and PRRT2-KO cultures, before and after treatment with of 1 nM phrixotoxin-3 and 10 nM 4,9-anhydrotetrodotoxin. **B.** Average network burst (NB) frequencies measured for the two groups under basal conditions and after drug treatment. Data are means ± sem (N = 9 and 10 WT and PRRT2-KO neurons, respectively). *$p < 0.05$; **$p < 0.01$; one-way ANOVA/Bonferroni's tests.